Research Article

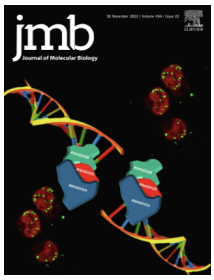

Fine-tuning of the Hsc70-based Human Protein Disaggregase Machinery by the Distinctive C-terminal Extension of Apg2

Yovana Cabrera [1†], Ganeko Bernardo-Seisdedos [3], Leire Dublang [1], David Albesa-Jové [1,3], Natalia Orozco [4], Ana Rosa Viguera [1], Oscar Millet [2], Arturo Muga [1] and Fernando Moro [1*]

*1 - **Instituto Biofisika (UPV/EHU,** CSIC) y Dpto. de Bioquímica y Biología Molecular, Facultad de Ciencia y Tecnología, Universidad del País Vasco, Barrio Sarriena S/N, 48940 Leioa, Spain*

*2 - **Precision Medicine and Metabolism Lab,** CIC bioGUNE, Bizkaia Technology Park, 48160 Derio, Spain*

*3 - **Ikerbasque,** Basque Foundation for Science, 48013 Bilbao, Spain*

*4 - **Fundación Biofísica Bizkaia,** Barrio Sarriena S/N, 48940 Leioa, Spain*

Correspondence to Fernando Moro: *Instituto Biofisika (UPV/EHU, CSIC) y Dpto. de Bioquímica y Biología Molecular, Facultad de Ciencia y Tecnología, Universidad del País Vasco, Barrio Sarriena S/N, 48940 Leioa, Spain. *fernando.moro@ehu.es* *(F. Moro)*

https://doi.org/10.1016/j.jmb.2022.167841

Edited by J. Buchner

Abstract

Apg2, one of the three cytosolic Hsp110 chaperones in humans, supports reactivation of unordered and ordered protein aggregates by Hsc70 (HspA8). Together with DnaJB1, Apg2 serves to nucleate Hsc70 molecules into sites where productive entropic pulling forces can be developed. During aggregate reactivation, Apg2 performs as a specialized nucleotide exchange factor, but the origin of its specialization is poorly defined. Here we report on the role of the distinctive C-terminal extension present in Apg2 and other metazoan homologs. We found that the first part of this Apg2 subdomain, with propensity to adopt α-helical structure, interacts with the nucleotide binding domain of Hsc70 in a nucleotide-dependent manner, contributing significantly to the stability of the Hsc70:Apg2 complex. Moreover, the second intrinsically disordered segment of Apg2 C-terminal extension plays an important role as a down-regulator of nucleotide exchange. An NMR analysis showed that the interaction with Hsc70 nucleotide binding domain modifies the chemical environment of residues located in important functional sites such as the interface between lobe I and II and the nucleotide binding site. Our data indicate that Apg2 C-terminal extension is a fine-tuner of human Hsc70 activity that optimizes the substrate remodeling ability of the chaperone system.

Introduction

The Hsp110 chaperone family in humans is constituted by three cytosolic/nuclear proteins, Hsp105, Apg1 and Apg2, and Grp170 in the ER lumen[1]. Together with Hsp70 and Hsp40 chaperones, Hsp110 proteins are part of the cellular protein homeostasis network[2]. Among other poorly characterized functions,[3] they suppress protein aggregation *in vivo* and *in vitro*[4–6]. The best characterized canonical role played by Hsp110s is the stimulation of ADP/ATP exchange in Hsp70 partners[7–8]. Human Apg2, as well as other Hsp110 from metazoans, are able to potentiate the efficient

refolding of protein aggregates by Hsp70 and Hsp40 chaperones[9–10]. Although Apg2 interacts very poorly with the aggregate, it significantly increases the amount of Hsc70 (HspA8), the constitutive human Hsp70, bound to the aggregate surface[11], but its precise role in the solubilization of polypeptide chains is not yet fully understood. The current hypothesis is that Apg2 acts as specialized nucleotide exchange factor (NEF) to stimulate protein aggregate reactivation[12], in contrast to other eukaryotic NEFs unable to support it, as Bag1.[9–10] It has been recently suggested that when dealing with ordered amyloids, the excluded volume effect imposed by the large molecular size of Apg2 promotes the selective dissociation of Hsc70 molecules sparsely bound to the amyloid surface and their reshuffling to more crowded sites, where productive entropic pulling forces can take place.[13–14]

Hsp110 proteins belong to the Hsp70 superfamily, sharing sequence and structural homology. The common domain organization of Hsp70 and Hsp110 proteins consists of an N-terminal nucleotide binding domain (NBD), able to hydrolyze ATP, and a C-terminal substrate binding domain (SBD), divided in a β-sandwich subdomain that holds the binding site for polypeptides (SBDβ) and a α-helical subdomain (SBDα) (Figure 1(A)). Despite the homology between these two chaperones, Hsp110s lack an Hsp70-like conformational cycle.[15–16] In Hsp110, the SBDβ and the SBDα dock on the NBD,[17] in a conformation resembling the ATP state of Hsp70s.[18] Distinctively, Hsp110s contain two sequence elongations: a subdomain rich in acidic residues inserted in the SBDβ (AS) and a C-terminal extension following the SBDα (Figure 1(A)). It is interesting to note here that these subdomains also distinguish Hsp110s from animal origin, such as human Apg2, from those of other organisms, such as yeast Sse1, in which both subdomains are shorter.[3] In order to understand the specialized function of Apg2 supporting protein aggregate reactivation, it is important to characterize the role played by these two distinctive subdomains. We previously found that the AS of Apg2 is important to regulate the chaperone cycle of Hsc70, acting as a molecular switch to facilitate dissociation of Hsc70:Apg2 complexes, avoiding their unproductive reassociation possibly through its interaction with Hsc70 SBD.[11] This allows the Hsc70 system to be active over a wider range of Apg2 concentrations.[11] Both divergent domains are involved in the physiological localization in the cytosol and the nucleus of mouse Hsp105α and Hsp105β, two isoforms formed by alternative splicing of a segment in the AS, also present in humans.[19–20] Recently, it has been shown that an

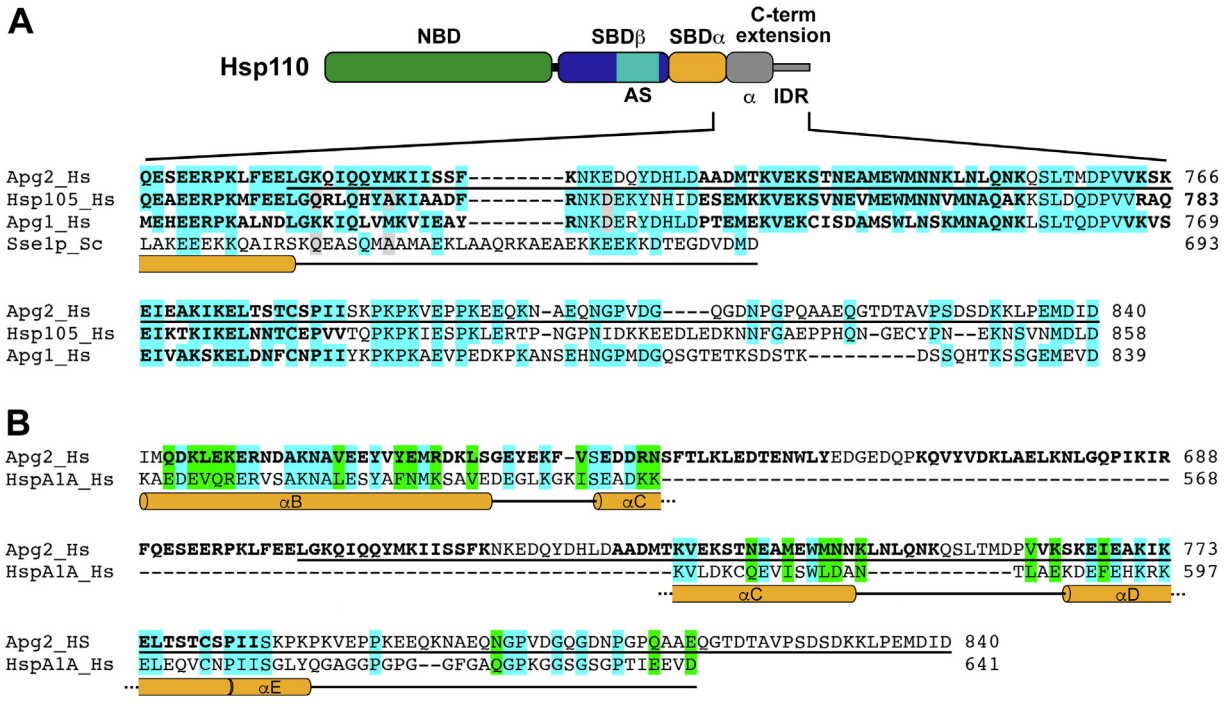

Figure 1. Properties of Apg2 C-terminal extension and the Apg2ΔC mutant. (**A**), the domain distribution scheme of human Hsp110 proteins and the sequence alignment of their C-terminal extensions, including yeast Sse1. The differentiated regions in the C-terminal extension are identified. Identical residues are highlighted in cyan. (**B**), Sequence alignment of human Apg2 and HspA1A. Cyan and green boxes highlight identical and similar residues, respectively. The C-terminal α-helix segments forming the 4-helix bundle lid of HspA1A are indicated underneath the sequence by orange cylinders. In A and B, the sequence deleted in Apg2ΔC is underlined and the residues in bold present a high probability to adopt an α-helical conformation according to Jpred4 prediction.

intrinsically disordered region in the C-terminal extension of *Drosophila melanogaster* Hsc70Cb, as well as human Apg1 and Hsp105, inhibits the formation of amyloid fibrils *in vitro*[21]. The C-terminal extension is also the target of several post-translational modifications, as phosphorylation[22] and ubiquitylation,[23–24] among others, that could have an important role regulating Apg2 activity in different physiological situations. However, it remains unknown how the C-terminal extension of human Hsp110s specifically affects the chaperone cycle of Hsp70 proteins and their substrate remodeling activity.

Here we have studied the role of the C-terminal extension of Apg2 in the interaction and regulation of Hsc70 activity, using two deletion mutants: one lacking the entire subdomain and a second one in which only the intrinsically disordered region was eliminated. First, we found that the structured segment of C-terminal extension is important to increase the affinity of Apg2 for Hsc70 in a nucleotide dependent manner. Second, an NMR analysis supports the involvement of the C-terminal extension of Apg2 in complex formation with Hsc70. Analysis of chemical shift perturbations revealed that Apg2 C-terminus affects key points in the interface between subdomains IB and IIB. Finally, the intrinsically disordered region decelerates the Apg2-induced stimulation of nucleotide exchange in Hsc70 and regulates the substrate remodeling ability of the chaperone system. This work, together with our previous study of the role played by the AS,[11] shows that the divergent domains in Apg2 finely tune the chaperone activity of the Hsc70 system.

Results

Conformational characteristics of the C-terminal extension and the Apg2ΔC mutant

We constructed a deletion mutant of human Apg2 lacking the last 139 residues, from L702 to D840, named Apg2ΔC, to investigate the role of the protein C-terminal extension (Figure 1(A)). This deletion site was chosen to match the last structured α-helical segment in the SBDα of the yeast homolog Sse1. The deleted sequence has hydrophilic character, is rich in acidic residues and is well conserved among human Hsp110s, especially its first half, in contrast to the shorter C-terminal extension of the yeast homolog Sse1 (Figure 1(A)). A Jpred4[25] secondary structure prediction showed high propensity to adopt helical structures for the conserved initial part of the C-terminal extension (Figure 1(A), residues in bold), while the last segment is predicted to be intrinsically disordered.[26] Moreover, the sequence alignment between Apg2 and HspA1A showed that the helical bundle formed by helices αC, αD and αE in the latter[27] has homology with segments in the first part of the Apg2 C-terminal extension (Figure 1(B)). The loss in molar ellipticity of the negative peaks at 208 and 222 nm observed in the far-UV circular dichroism spectrum of Apg2ΔC compared to the wt protein, indicated a lower helical content in the mutant, in agreement with the above predictions (Figure 2(A)).

In order to check the folding integrity of Apg2ΔC, we performed small-angle X-ray scattering (SAXS) measurements and partial trypsin proteolysis. The comparison between the structural parameters derived from wt Apg2[11] and Apg2ΔC provided strong evidences that Apg2ΔC folded as a compact protein (Figure 2(B)). The molecular mass estimated from the Volume-of-correlation (V_c) of Apg2ΔC was 83 kDa (Supplemental Table 1), which approximates the 79 kDa calculated from Apg2ΔC sequence. Furthermore, the expected reduction of 15 kDa in the molecular mass upon deletion of the C-terminal extension of Apg2, estimated from the protein sequence, reasonably agreed with the 13 kDa loss determined from the V_c values of Apg2ΔC (83 kDa) and Apg2 (96 kDa).[11] Importantly, comparison between the radius of gyration (R_g) and the maximum distance (D_{max}) parameters of Apg2ΔC and Apg2 clearly indicate that Apg2ΔC is a more compact particle ($\Delta D_{max\ (Apg2\ -\ Apg2\Delta C)}$ = 28 Å, $\Delta R_{g\ (Apg2\ -\ Apg2\Delta C)}$ = 8.3 to 8.7 Å), which might be related to the lack of the predicted intrinsically disordered C-terminal segment.[26] The *ab-initio* reconstruction of Apg2ΔC showed an elongated envelope (Figure 2(B)), similar to that found for wt Apg2 but lacking its characteristic V-shape.[11] Using MONSA to simultaneously fit wt Apg2 and Apg2ΔC scattering curves allowed to predict the localization of the C-terminal extension occupying one lobe of the V-shaped envelope of the wt protein (Figure 2(C)). This position for the C-terminal extension is in agreement with our 3D atomistic model[11], and very similar to the AlphaFold prediction.[28–29]

Using partial proteolysis, we found that both wt Apg2 and Apg2ΔC adopted a similar conformation as they were degraded by trypsin to a fragment of approximately 66 kDa with similar kinetics, regardless of the presence of nucleotides (Supplemental Figure S1(A) and (B)). Taken together, these results show that Apg2ΔC adopts a folded, anisotropic and compact conformation. They also suggest that part of C-terminal extension of Apg2 possibly adopts an α-helical conformation that could enlarge the helical bundle in the SBDα.

The C-terminal extension is required to induce a high affinity state of the Hsc70:Apg2 complex in the presence of nucleotides

Since the α-helical bundle and C-terminal region of Sse1 are important elements in the interaction with Ssa1, its Hsp70 partner in yeast,[7,30] we investigated how the deletion of Apg2 C-terminal extension affected complex formation with Hsc70.

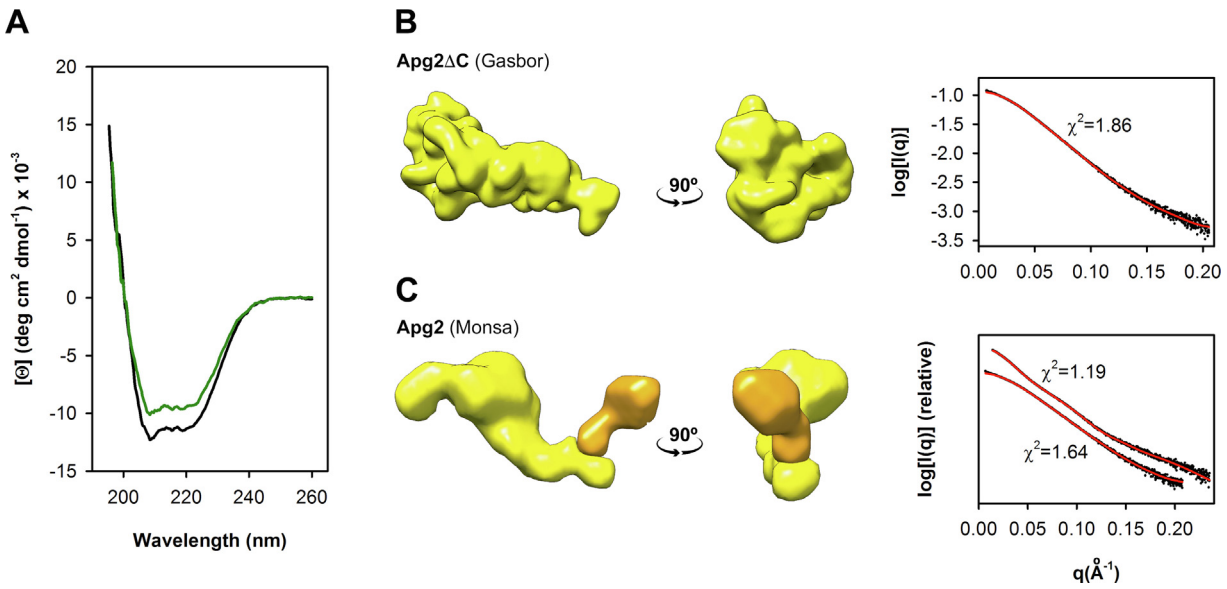

Figure 2. Conformational properties of Apg2ΔC. (**A**), Far-UV circular dichroism spectra of wt Apg2 (black line) and Apg2ΔC (green line) in the absence of nucleotides. 10 spectra were recorded and averaged in JASCO J-8100 spectropolarimeter (Jasco, Tokio, Japan), using a 1 mm path length cuvette. Protein concentration was 2.5 μM. (**B**), two views of the *ab-initio* envelope reconstruction of Apg2ΔC using GASBOR. Right panel shows SAXS data and the fitting to the predicted envelope (x^2 is given). (**C**), Reconstruction of wt Apg2 envelope using MONSA, which simultaneously fits Apg2ΔC and Apg2 SAXS data. SAXS data for wt Apg2 were taken from Cabrera et al.[11]. Phases Apg2ΔC (yellow) and C-terminal extension (orange) were defined in MONSA reconstruction. The SAXS curves and the corresponding fittings are shown on the right panel.

These experiments were performed in conditions that allow formation of stable complexes in equilibrium: when both proteins are in apo conformation or after a long incubation in the presence of ATP[11]. First, the equilibrium binding constants in the absence of nucleotides were determined by SPR.[11] Briefly, Hsc70 carrying a C-terminal strep-tag was bound to a CM5 chip in which an anti-streptag antibody was immobilized, and successive injections of Apg2 or Apg2ΔC were performed to record the sensorgrams (Supplementary Figure S2(A)). Apg2ΔC bound to Hsc70 with fast association and dissociation kinetics, similarly to what was found for wt Apg2 and Sse1.[11,31] Dissociation constants (K_d) were derived from plots of the maximal RUs against Hsp110 concentration (Supplementary Figure S2(B)), resulting in values of 148 ± 5 nM for Apg2 and 151 ± 16 nM for Apg2ΔC. Thus, deletion of Apg2 C-terminal extension did not affect the affinity for Hsc70 in the absence of nucleotides. As a control of the chaperone's functionality, Apg2ΔC did not bind to immobilized Hsc70 in the presence of ATP, as we found for wt Apg2[11]. However, a long incubation in the presence of ATP, allowing complete hydrolysis of the nucleotide, resulted in formation of a complex that could be resolved by size exclusion chromatography or native electrophoresis[11]. This, together with the observed lack of interaction between ATP-bound Apg2 and Hsc70 and the low affinity in the presence of ADP[11], led us to suggest the formation of Hsc70:Apg2 asymmetric complexes regarding the nucleotide state of each protein, i.e., Apg2 would be bound to ATP while Hsc70 would contain ADP or be in apo conformation[11]. This interpretation agrees with the crystallized complexes of Sse1 with Ssa1[30] or bovine Hsc70.[32] In the first one, Sse1 is bound to ATP while Ssa1 is in the apo state, and in the second Sse1 contains ADP*BeF_x, a complex that mimics ATP effects,[33–34] whereas Hsc70 is ADP-bound. Unfortunately, the nucleotide asymmetry in the complex precludes the use of direct experimental methods, like SPR, to estimate the complex affinity.

We sought to study Apg2 and Apg2ΔC association to Hsc70 estimating the amount of complex formed after extensive ATP hydrolysis by native gel electrophoresis (Figure 3). Initial scouting experiments showed a strong affinity of Apg2 for Hsc70 with a K_d in the order of that found by SPR or lower, which represents a challenge since concentrations of the titrating protein (typically Apg2) close or below the detection limit should be used. To circumvent this limitation and taking advantage of the fact that the complexes of Hsc70 with Apg2 and Apg2ΔC could be resolved by native gels (Figure 3(A) and (C), lane 2), we performed competition experiments between Apg2 and Apg2ΔC to bind Hsc70. Two competition assays were carried out: in the first one, Hsc70 (2 μM) was incubated with wt Apg2 (2 μM constant) and increasing concentrations of Apg2ΔC (Figure 3(A)), while in the second one,

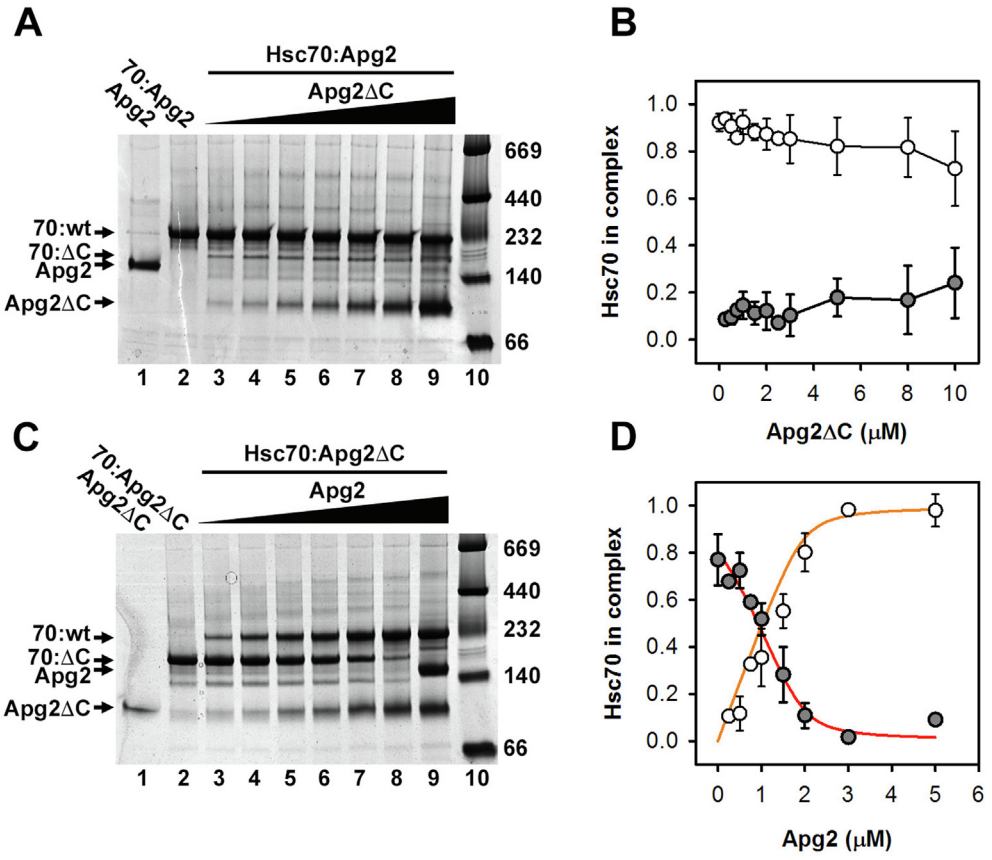

Figure 3. Competitive binding of Apg2 and Apg2ΔC to Hsc70 in the presence of nucleotides analyzed by native electrophoresis. (**A**), native electrophoresis of wild-type Apg2 (2 μM, lane 1), the Hsc70:Apg2 complex (2 μM each protein, lane 2) and the competition assay at increasing Apg2ΔC (from lane 3: 0.25, 0.5, 0.75, 1, 1.5, 2, and 5 μM), and constant Apg2 concentration (2 μM). Proteins were incubated overnight at 25 °C in the presence of 50 μM ATP. Molecular weight markers are shown in lane 10. (**B**), fraction of Hsc70 bound to Apg2 (white circles) or Apg2ΔC (gray circles) estimated from competition assays performed as in A. Note that a concentration range from 0 to 10 μM Apg2ΔC was scanned in different competition assays and not all gels included the concentrations shown in A. (**C**), native electrophoresis of Apg2ΔC (2 μM, lane 1), the Hsc70:Apg2ΔC complex (2 μM each protein, lane 2) and the competition assay at increasing Apg2 (from lane 3: 0.25, 0.5, 0.75, 1, 1.5, 2, and 5 μM) and constant Apg2ΔC concentration (2 μM). Molecular weight markers are shown in lane 10. (**D**), fraction of Hsc70 bound to Apg2 (white circles) or Apg2ΔC (gray circles) derived from competition assays performed as in C. The red line represents the best fit of the experimental data to a competitive binding model[35], resulting in K_d values of 2 ± 1 nM and 100 ± 35 nM for Apg2 and Apg2ΔC, respectively. The orange line was calculated using these K_d values. In B and D, the average and standard deviations of four independent experiments are shown.

Apg2ΔC was kept constant at 2 μM and wt Apg2 concentration was increased (Figure 3(C)). We observed that Apg2ΔC could not outcompete wt Apg2 to bind Hsc70 (Figure 3(A)), and only a minor fraction of Hsc70 bound to the mutant when its concentration was above 5 μM (Figure 3(B)). On the other hand, Apg2 competed very efficiently with Apg2ΔC to bind Hsc70, even at the lowest concentrations of the wt protein tested (Figure 3 (C)). As a reference, practically the majority of Hsc70 was bound to Apg2 in lane 8 of both gels, corresponding to the equimolar mixture of Apg2, Apg2ΔC and Hsc70 (2 μM each). From these experiments, it is clear that there is a large affinity difference between Apg2 and Apg2ΔC for Hsc70 in the presence of nucleotides, in contrast to the apo conditions. Therefore, the C-terminal extension is an element that contributes significantly to increase the stability of the nucleotide bound Hsc70:Apg2 complex.

The fact that the complexes of Hsc70 with wt Apg2 and Apg2ΔC could be resolved, aimed us to estimate the equilibrium dissociation constants for both complexes. For this, competition assays as that shown in Figure 2C, where Hsc70 gradually switched from a complex with Apg2ΔC to a complex with wt Apg2, were analyzed. This type of experiments can be defined by two equilibria and the corresponding equilibrium dissociation constants:

$$\mathrm{Hsc70} + \mathrm{Apg2} \rightleftarrows \mathrm{Hsc70} : \mathrm{Apg2}$$

$$K_d^{wt} = \frac{[Hsc70][Apg2]}{[Hsc70 : Apg2]} \quad (1)$$

$$\mathrm{Hsc70} + \mathrm{Apg2\Delta C} \rightleftarrows \mathrm{Hsc70} : \mathrm{Apg2\Delta C}$$

$$K_d^{\Delta C} = \frac{[Hsc70][Apg2\Delta C]}{Hsc70 : Apg2\Delta C} \quad (2)$$

where the mass conservation equations are:

$$[Apg2]_{tot} = [Apg2] + [Hsc70 : Apg2] \quad (3)$$

$$[Apg2\Delta C]_{tot} = [Apg2\Delta C] + [Hsc70 : Apg2\Delta C] \quad (4)$$

$$[Hsc70]_{tot} = [Hsc70] + [Hsc70 : Apg2] + [Hsc70 : Apg2\Delta C] \quad (5)$$

from Eq. (1), (2), (3) and (4):

$$[Hsc70 : Apg2] = \frac{[Apg2]_{tot}[Hsc70]}{K_d^{wt} + [Hsc70]}$$

$$[Hsc70 : Apg2\Delta C] = \frac{[Apg2\Delta C]_{tot}[Hsc70]}{K_d^{\Delta C} + [Hsc70]}$$

Substituting these expressions into Eq. (5) resulted in a cubic equation (Eq. (6)) that relates the concentration of free Hsc70 as a function of K_d^{wt}, $K_d^{\Delta C}$ and the total concentrations of Hsc70, Apg2 and Apg2ΔC:

$$0 = [Hsc70]([Hsc70]^2 + A[Hsc70] + B) - K_d^{wt}K_d^{\Delta C}[Hsc70]_{tot} \quad (6)$$

where

$$A = K_d^{wt} + K_d^{\Delta C} + [Apg2]_{tot} + [Apg2\Delta C]_{tot} - [Hsc70]_{tot}$$

$$B = K_d^{wt}K_d^{\Delta C} + K_d^{wt}([Apg2\Delta C]_{tot} - [Hsc70]_{tot}) + K_d^{\Delta C}([Apg2]_{tot} - [Hsc70]_{tot})$$

The solution to this equation,[35] was used to fit the data obtained by densitometry of four independent assays (Figure 3(D)). The best fit was obtained with values of 2 ± 1 nM for K_d^{wt} and 100 ± 35 nM for $K_d^{\Delta C}$. Although these values should be taken with caution due to the experimental method used, they clearly demonstrate that Apg2 C-terminal extension strongly contributes to complex formation with Hsc70 in the presence of nucleotides, enhancing the affinity between 1 and 2 orders of magnitude. Moreover, taking into account that Apg2 and Apg2ΔC interacted similarly with Hsc70 in the absence of nucleotides, this strong affinity difference in the presence of nucleotides suggests that the C-terminal extension of Apg2 is sensitive to the nucleotide-induced conformational rearrangement of the chaperones. However, no significant differences were detected between apo, ADP and ATP conformations of Apg2 and Apg2ΔC when we tested conformational changes upon nucleotide binding by limited proteolysis (Supplementary Figure S1), in good agreement with other reports.[15] In order to get a better insight into ATP-induced conformational changes in Apg2, we resorted to differential infrared spectroscopy (IR).[36–37] These experiments revealed the insensibility of Apg2 to ATP binding, in contrast to Hsc70 which showed a characteristic differential IR spectrum that resembled that of DnaK,[37] with clear differential signals that could be attributed to ATP-induced conformational changes (Supplemental Figure S1(C)). These results bring up the possibility that the rearrangement of Apg2 C-terminal region depends on the binding of both ATP and Hsc70(ADP) to the cochaperone.

Apg2 C-terminal extension interacts with lobe I and II of Hsc70 NBD

To study in more detail the role of Apg2 C-terminal extension in complex formation with Hsc70, we performed a chemical shift perturbation (CSP) analysis by NMR. As revealed in the crystal structures of the homolog Sse1 complexed with two different Hsp70 proteins,[30,32] the C-terminal helical bundle in the SBDα of Sse1 interacts directly with lobe II of Hsp70 NBD. By homology, this positions the C-terminal extension of Apg2 in close proximity to Hsc70 NBD, making both protein regions good candidates to establish an intermolecular interaction. To find out if this was the case, the NBD of Hsc70 (150 μM), labelled with ^{15}N, was mixed with substoichiometric concentrations of Apg2 or Apg2ΔC (75 μM) in the presence of 500 μM ATP and incubated for 12 h at room temperature before NMR measurements. Backbone chemical shifts were assigned based on BMRB entry 26815[38] (Supplementary Figure S3(A)).

As expected, Apg2 and Apg2ΔC binding produced chemical shift perturbations and changes in the correlation time that resulted in signal broadening, and a consequent reduction in peak intensity of Hsc70 NBD protein signals (Supplementary Figure S3(B)). The chemical environment of specific Hsc70 residues located in contact sites with Apg2 was modified by both wt Apg2 and Apg2ΔC (Figure 4(A), greyed areas). These sites were inferred by homology with the complex of yeast Sse1 with bovine Hsc70[32] and yeast Ssa1.[30] For instance, we observed chemical shifts in L135 and R299 (Figure 4(B)), two residues located in the vicinity of Hsp110 NBD and SBDα, respectively (Figure 4(D)). Line broadening over these signals is distinctively observed upon interaction with both Apg2 variants, the effect being stronger for the wt protein. Especially interesting in the context of this work are those resonances that were significantly modified by Apg2 (shifted or lost due to signal broadening), but were barely affected by Apg2ΔC (Figure 4(A), red bars and blue dots). To explore these signals, we selected residues whose signal was lost or had a CSP value higher than 0.02 for the complex with wt Apg2, while having a CSP lower than 0.008 in the complex with Apg2ΔC (Figure 4(C) shows two examples). These residues are located in subdomain IIA, right next to Apg2 SBDα,

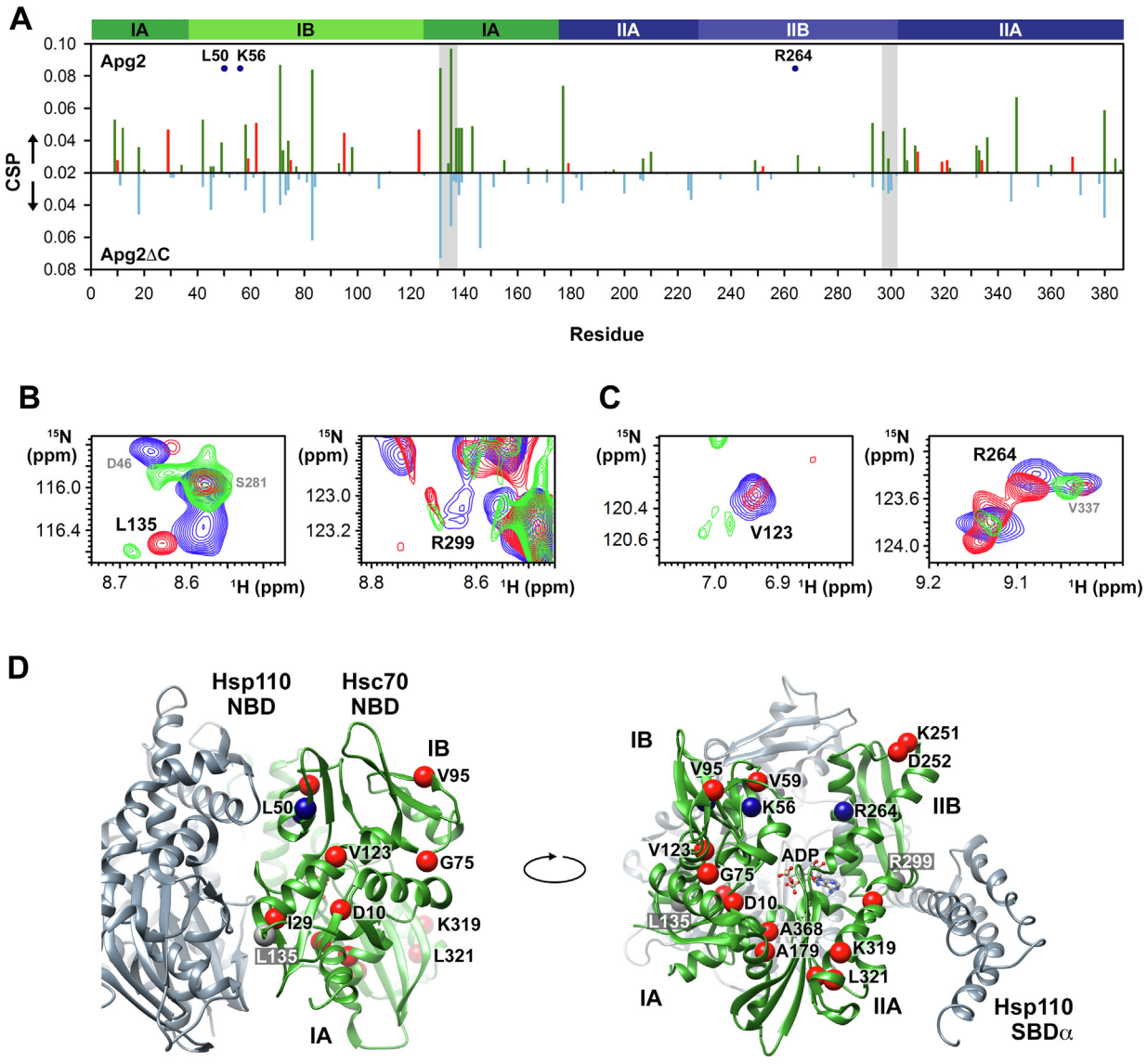

Figure 4. NMR analysis of Apg2 and Apg2ΔC binding to Hsc70 NBD. (**A**), chemical shift perturbation (CSP) values obtained after incubating 150 μM Hsc70 NBD and 75 μM wt Apg2 (upper panel, green bars) or Apg2ΔC (lower panel, blue bars). A threshold of 0.02 was used in order to reduce noise. Greyed areas indicate contact sites between Apg2 and Hsc70, expected by homology with the complexes of yeast Sse1 with Hsp70 proteins[30,32]. Residues barely affected by Apg2ΔC (CSP $\leq$ 0.008) but with a significant chemical shift (CSP $\geq$ 0.02, red bars) in the complex with wt Apg2 or whose resonance was lost due to signal broadening (labeled blue dots) were selected. (**B**), blown-up regions of the ^{1}H-^{15}N TROSY spectra showing the resonances of L135 (left) and R299 (right), two residues localized in contact sites. Blue lines correspond to the spectra obtained for the isolated Hsc70 NBD, green to the complex with wt Apg2 and red to the complex with Apg2ΔC. (**C**), two examples of residues that were significantly modified by Apg2 but not by Apg2ΔC, V123 (left) and R264 (right). Color code as in B. (**D**), Location of residues significantly modified in the complex with wt Apg2, but not with Apg2ΔC, in the structure of the ADP-bound NBD of bovine Hsc70 in complex with yeast Sse1 (pdb code 3c7n)[32]. Residues are shown in red and blue spheres according to the selection performed in A. Grey spheres and labels represent residues in B, located in contact sites. ADP is shown in ball and sticks representation.

and subdomains IA, IB, and IIB in Hsc70 NBD (Figure 4(D)). Interestingly, wt Apg2 modified the environment of residues in functionally relevant regions of Hsc70 NBD (Figure 4(D)), as: 1) the interface between subdomains IB (K56 and the neighboring V59) and IIB (R264), that might be important for nucleotide binding and exchange[39]; 2) the nucleotide binding site (D10); 3) a hinge in subdomain IB (G75)[40] and the connecting helix with subdomain IA (V123); and 4) the hydrophobic

groove that serves as docking site for the Hsc70 linker in the ATP conformation and the J-domain of Hsp40 proteins (A179 and A368).[18,41–42] Some residues were localized buried from solvent in the complex, as I29 and L50 in the interface between the NBDs of Hsc70 and Apg2 (Figure 4(D), left image) or D10 in the nucleotide binding site, among others, which possibly indicates that deletion of the C-terminal extension allosterically modified their environment. Another group of residues showing large CSPs in the complex with wt Apg2, as G75, V95, K319 and L321, was located in the exposed face of Hsc70 NBD, opposed to Apg2 NBD (Figure 4 (A) and (D)). Although allosteric effects cannot be completely discarded, modification in the environment of these exposed residues possibly suggests an interaction with Apg2 C-terminal extension. However, we cannot precisely map the binding site due to the severe signal broadening observed. Nevertheless, the differences in CSPs of key Hsc70 NBD residues found between its complex with wt Apg2 or Apg2ΔC further support the involvement of the C-terminal extension in Hsc70 binding.

Nucleotide exchange is regulated by the IDR in Apg2 C-terminal extension

The interaction of Apg2 C-terminal extension with both lobes of Hsc70 NBD revealed by NMR suggests that it might modulate nucleotide exchange. The release of the fluorescent nucleotide analog MABA-ADP from Hsc70 was followed in a stopped-flow device by mixing the preformed Hsc70(MABA-ADP) complex (0.5 μM) with 250 μM ATP and increasing concentrations of Apg2 and Apg2ΔC. To avoid unwanted hydrolysis of ATP, Hsp110 concentration was kept below 0.4 μM and ATP was injected from a separate syringe and premixed with the corresponding Hsp110 for 5 s before the final mixing with Hsc70 (MABA-ADP). At 0.1 μM, Apg2 promoted nucleotide exchange at 0.59 s^{-1}, 3-fold faster that the spontaneous exchange observed in its absence (Figure 5(A)). In the same conditions, the mutant Apg2ΔC exchanged the nucleotide bound to Hsc70 at 1.08 s^{-1} (Figure 5(A)), almost 2-fold faster than the wt protein. Titration of Apg2 and Apg2ΔC showed that the deletion mutant induced, on average, a 1.6-fold faster nucleotide exchange reaction in the concentration range tested (Figure 5(B)). To get a deeper insight into the role played by the C-terminal extension in nucleotide exchange, we constructed a mutant in which only the intrinsically disordered region was deleted (including residues from P781 to D840). This mutant, named Apg2ΔIDR, promoted nucleotide exchange in Hsc70 similarly to Apg2ΔC (Figure 5 (B)), revealing the IDR in Apg2 C-terminal extension as a functional regulator of Hsc70 cycle.

The results presented above show that Apg2ΔC and Apg2ΔIDR are more efficient NEFs for Hsc70 than wt Apg2. Then, we wondered if this

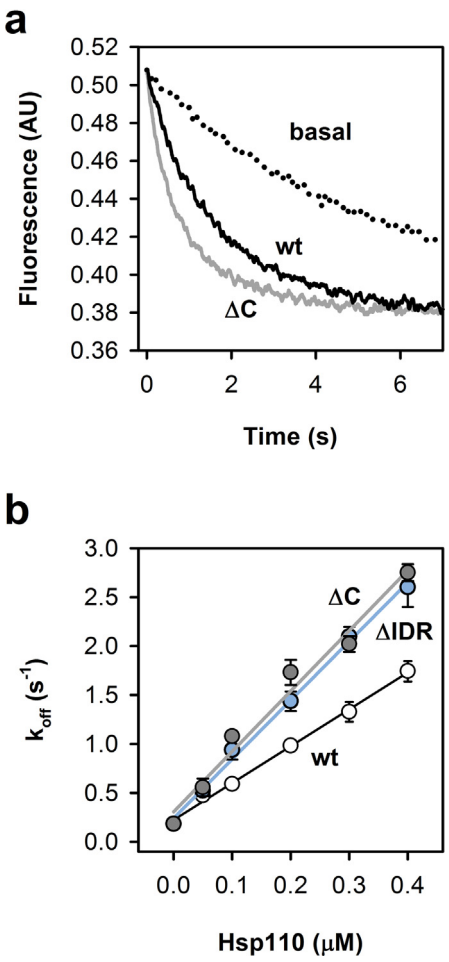

Figure 5. The IDR in Apg2 C-terminal extension down regulates nucleotide exchange in Hsc70. (**A**), dissociation of MABA-ADP from Hsc70 monitored in a stopped-flow device as a decrease in fluorescence intensity upon addition of ATP (dotted line), ATP and Apg2 (black line), or ATP and Apg2ΔC (grey line). Apg2 and Apg2ΔC were 0.1 μM. (**B**), apparent dissociation constants (k_{off}) of MABA-ADP bound to Hsc70 at increasing concentrations of Apg2 (open circles), Apg2ΔC (grey circles) and Apg2ΔIDR (blue circles). Observed k_{off} constants were obtained after fitting the time course of fluorescence intensity to a single exponential decay. Values are the average of three independent measurements.

difference in nucleotide exchange activity after partial or total deletion of the C-terminal extension might have other functional effects. We first measured the ATP hydrolysis rates of mixtures of Hsc70 with Apg2 or Apg2ΔC in the presence of DnaJB1 (Figure 6(A)). As in a previous work,[11] we analyzed the results using ΔATPase values obtained after subtraction of isolated Apg2 or Apg2ΔC ATPase from the total activity of the chaperone mixture, in order to eliminate the contribution of increasing Hsp110 concentration. We found that ΔATPase values for Apg2ΔC (Figure 6(A)) and

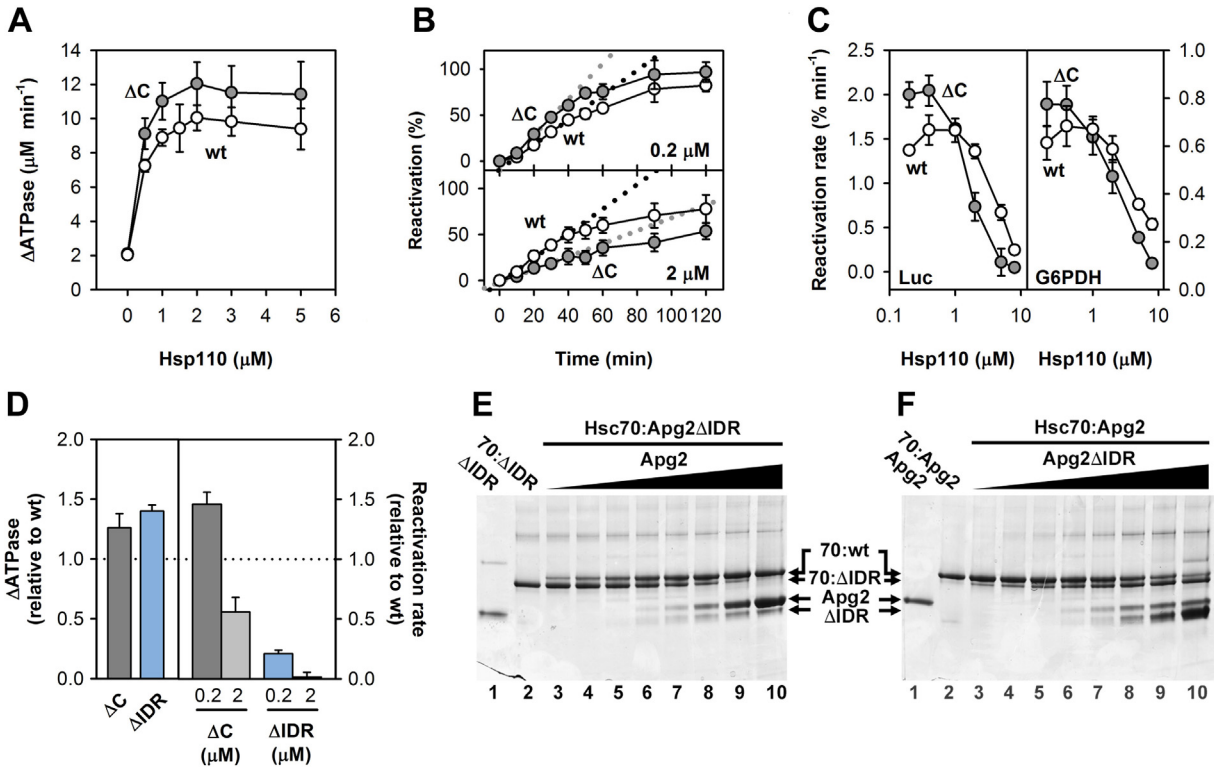

Figure 6. Functional consequences of the accelerated nucleotide exchange activity of Apg2ΔC and Apg2ΔIDR. (**A**), ΔATPase values of samples containing Hsc70 (2 μM), DnaJB1 (0.5 μM) and increasing concentrations of Apg2 (white symbols) or Apg2ΔC (grey symbols). (**B**), refolding time course of luciferase aggregates (20 nM) by Hsc70 (2 μM), DnaJB1 (1 μM) and Apg2 (white symbols) or Apg2ΔC (grey symbols) at 0.2 (upper panel) and 2 μM (lower panel). Dotted lines represent the linear regression of the initial points used to obtain the reactivation rate (black, wt; grey, Apg2ΔC). (**C**), dependence of the reactivation rate of luciferase and G6PDH aggregates on the concentration of Apg2 (white symbols) or Apg2ΔC (grey symbols). Average values and standard deviations of at least three independent assays are shown in A, B and C. (**D**), (left panel) ΔATPase values of 2 μM Hsc70 in the presence of 0.5 μM DnaJB1 and 0.5 μM Apg2ΔC (grey bar) or Apg2ΔIDR (blue bar), expressed relative to those obtained for wt Apg2. (Right panel) refolding rates of luciferase aggregates (relative to wt Apg2) obtained at 0.2 and 2 μM Apg2ΔC (grey bars) or Apg2ΔIDR (blue bars). (**E**), analysis by native electrophoresis of Apg2ΔIDR (2 μM, lane 1), its complex with Hsc70 (2 μM each protein, lane 2) and the competition assay at increasing wt Apg2 concentration (from lane 3: 0.5, 0.75, 1, 1.5, 2, 3, 5 and 10 μM) while keeping constant 2 μM Apg2ΔIDR. Proteins were incubated overnight at 25 °C in the presence of 50 μM ATP. (**F**), Apg2 (2 μM, lane 1), the Hsc70:Apg2 complex (2 μM each protein, lane 2) and the competition assay at increasing Apg2ΔIDR (from lane 3: 0.5, 0.75, 1, 1.5, 2, 3, 5 and 10 μM) and constant 2 μM Apg2 analyzed by native gels.

Apg2ΔIDR (Figure 6(D)) were 20–30 % higher than for wt Apg2, which correlated with the higher nucleotide exchange activity of the mutants. Second, we tested the refolding of protein aggregates by Hsc70 and DnaJB1 assisted by wt Apg2 or the two C-terminal deletion mutants. Compared to wt Apg2, Apg2ΔC promoted a 45 % faster reactivation of luciferase aggregates at 0.2 μM (Figure 6(B)), with initial reaction kinetics of 2.0 % min^{-1} for the mutant and 1.37 % min^{-1} for the wt protein. However, raising the concentration of Apg2ΔC to 2 μM inhibited the refolding activity to 0.73 % min^{-1}, a 45 % slower rate than that obtained for wt Apg2. Titration of wt Apg2 and Apg2ΔC showed that luciferase and glucose-6-phosphate dehydrogenase (G6PDH) aggregates were reactivated faster in the presence of the mutant below 1 μM (Figure 6 (C)). Above this concentration, the refolding activity diminished faster for Apg2ΔC than for wt Apg2. These results suggests that refolding of protein aggregates in the presence of Apg2ΔC was affected by its accelerated nucleotide exchange activity. In contrast to Apg2ΔC, Apg2ΔIDR exhibited a strong inhibition of protein reactivation, as recovery of luciferase aggregates was reduced to 20 % of the amount refolded in the presence of wt Apg2 at 0.2 μM, and almost abolished at 2 μM (Figure 6 (D)). In order to understand the different behavior of the two C-terminal deletion mutans in protein refolding, we studied the affinity of Apg2ΔIDR for Hsc70 in the presence of nucleotides following the procedure described above for Apg2ΔC. As

expected, increasing concentrations of wt Apg2 could compete with Apg2ΔIDR to bind Hsc70 (Figure 6(E)), but, differently to Apg2ΔC (see Figure 3 (A)), Apg2ΔIDR could also compete with wt Apg2, sequestering Hsc70 in the concentration range used (Figure 6(F)). At 2 μM Apg2 and Apg2ΔIDR (line 7), Hsc70 distributed in complexes with both Apg2 proteins, although the complex with the wt slightly predominated. This indicates that Apg2-ΔIDR has a higher affinity for Hsc70 than Apg2ΔC, closer to that of the wt protein. Quantification and fitting of the native gels showed that the dissociation constant was increased approximately 2-fold compared to wt Apg2 (Supplemental Figure 4). Taken together, these results indicate that the disordered segment of Apg2 C-terminal domain plays an important role as a nucleotide exchange regulator, while the α-helical bundle is essential to form a high affinity complex with Hsc70 in the presence of nucleotides.

Discussion

We show herein that the C-terminal extension of Apg2 is an important regulatory element of the human Hsc70 chaperone system. This 150 residues elongation of the C-terminus following the SBDα is present in metazoan Hsp110 proteins, being shorter in homologs from fungi.[3,15] Apg2 C-terminal extension can be divided in two differentiated regions: a segment predicted to form a 3-helix bundle[11,28–29], well conserved in the other two human Hsp110 proteins (Hsp105 and Apg1), followed by a more divergent C-terminal intrinsically disordered region (IDR),[26] as also found for *Drosophila melanogaster* Hsc70Cb.[21] Using two Apg2 mutants, one without the entire C-terminal extension (Apg2ΔC) and a second in which only the intrinsically disordered segment was deleted (Apg2ΔIDR), we demonstrate that the 3-helix bundle segment enhances approximately 2 orders of magnitude the affinity of Apg2 for Hsc70 in the presence of nucleotides. Moreover, our data also show that the IDR regulates nucleotide exchange in Hsc70 and, hence, the chaperone activity of the system. Although specific effects of Apg1 and Hsp105 C-terminal extensions remain to be explored, significant differences with Apg2 are not expected given the similarity of the three human Hsp110 proteins in nucleotide exchange activity and the stimulation of protein aggregate reactivation by the Hsc70 system[9]. Instead, the C-terminal extension possibly contributes to differentiate human, or other metazoans, Hsp110s from those found in eukaryotic cells as yeast. Although Dragovic and coworkers[7] found that deletion of the last 44 C-terminal disordered residues of Sse1 also reduced the affinity for Hsp70, the Sse1 truncated mutant abolished nucleotide exchange *in vitro*,[7] in contrast to our result. However, the same Sse1 C-terminal deletion mutant was able to complement the temperature-sensitive phenotype of a *sse1*Δ yeast strain,[43] which points out that the precise role of Sse1 C-terminal segment is still poorly defined. When the refolding of luciferase aggregates by human Hsc70/DnaJB1/Apg2 and the yeast homologs Ssa1/Ydj1/Sse1 was compared, Rampelt *et al.* found the yeast system to be approximately 50% less active, requiring the presence of Hsp104, a protein belonging to the Hsp100 family, for full activation.[9] We suggest that the C-terminal extension in metazoan Hsp110 serves, together with other factors, to fine-tune the Hsc70 system in order to facilitate protein aggregate reactivation in organisms that lack Hsp100 proteins, as humans.

The increased nucleotide exchange activity of Apg2ΔC and Apg2ΔIDR is expected to accelerate the conformational cycle of Hsc70 associated to ATP binding and hydrolysis. Indeed, we found experimentally an increment in the ATPase activity of Hsc70 in the presence of DnaJB1 and both mutants compared to wt Apg2. Moreover, the disaggregase activity of the chaperone system was stronger with Apg2ΔC than with wt Apg2 at concentrations lower than 1 μM, where the faster nucleotide exchange in Hsc70 induced by the mutant might compensate its lower affinity and potentiate protein refolding. An increase in ADP/ATP exchange activity could be beneficial for protein refolding in situations where nucleotide exchange is limited, for instance, in the presence of inorganic phosphate.[44] Moreover, the expected inhibition of aggregate reactivation at elevated NEF concentration due to the detrimental effect of fast ADP/ATP exchange in refolding reactions,[11,44–46] occurred at lower NEF/Hsc70 ratios for Apg2ΔC than for wt Apg2, in agreement to the more potent NEF activity found for the mutant. However, the differences between wt Apg2 and Apg2ΔC in nucleotide exchange, Hsc70 ATPase stimulation and disaggregase activity of the chaperone system are rather subtle compared to the strong difference in affinity for Hsc70 between both proteins in the presence of nucleotides, indicating a role as a fine-tuner for the C-terminal extension. These functional assays were performed with ATP in excess, a more physiological condition, meaning that Apg2 and Apg2ΔC interacted dynamically with Hsc70. Therefore, the interaction is kinetically driven, which might result in a less pronounced effect of the C-terminal domain deletion than that observed for complex formation in equilibrium. The affinity difference with wt Apg2 could be due to a slower association or a faster dissociation (or both) of the Hsc70:Apg2ΔC complex. The formation/dissociation kinetics of the Hsc70:Apg2ΔC complex in the presence of ATP, combined with its higher nucleotide exchange activity, might diminish the functional differences with wt Apg2. On the other hand, the affin-

ity of Apg2ΔIDR for Hsc70 and, possibly, the kinetic constants regulating the interaction are much closer to those of wt Apg2, which results in the inhibition of the refolding activity of the Hsc70 system due to the elevated nucleotide exchange activity imposed by this mutant.

The NBD of Hsp70 proteins transmits a different allosteric signal to the SBD depending on the nucleotide bound.[41,47–48] Hsc70 NBD is formed by two lobes, I and II, divided in subdomains IA, IB and IIA and IIB (see Figure 4(B)), that form a nucleotide binding cleft where an ATP molecule is bound and hydrolyzed. ADP/ATP exchange is a key step in the functional cycle of Hsp70 that requires opening of the nucleotide binding cleft. Different open states are possibly part of the conformational landscape of the NBD[41], and specific NEFs select one in order to facilitate the process.[30,32,49–50] Yeast Hsp110, Sse1, promotes an open state in which subdomain IIB of Hsp70 is rotated 27° sideways, by a face-to-face interaction between the NBDs of both proteins and docking of Sse1 SBDα at lobe II of Hsp70.[30,32] Using NMR spectroscopy, we find here that the long C-terminal extension of Apg2 modifies the environment of residues located in both lobes of Hsc70 NBD. The number of the residues affected by Apg2 C-terminal extension and its wide distribution supports the significant contribution of this protein region to Hsc70 binding. Although not required for complex formation with Hsc70, as Apg2ΔC was also able to bind the chaperone, the C-terminal extension of Apg2 adds another layer of complexity to nucleotide exchange in the human Hsc70 system, where it could regulate the aperture degree of Hsc70 NBD. The high number of resonances modified in the CSP analysis complicates unveiling the precise mechanism used by the C-terminal extension to decelerate nucleotide exchange, but it is worthy to discuss the role of some residues relevant for the functionality of Hsc70 that are perturbed by wt Apg2 but not by Apg2ΔC. One of them is D10, located in the nucleotide binding site and involved in the correct positioning of Mg^{2+} and ATP γ-phosphate[51], resulting critical for ATP binding and hydrolysis.[52–53] Apg2-induced modification of D10 might slow down ADP release through the stabilization of the nucleotide in the post hydrolysis state (ADP + Pi). In line with this hypothesis, physiological concentrations of inorganic phosphate greatly decelerated ADP release from Hsp70 proteins, even in the presence of NEFs.[42,54,55] Two residues at the interface of the Hsc70 nucleotide binding cleft, K56 (subdomain IB) and R264 (subdomain IIB) were strongly modified by the C-terminal extension as their resonances were lost in the complex with wt Apg2, while they were not affected by Apg2ΔC. K56 is especially interesting as it might establish an ionic contact with E268 in lobe IIB[51]. This salt bridge between lobe I and lobe II is suggested to close the nucleotide binding cleft and control nucleotide dissociation.[39] Indeed, mutation of this residue promoted faster nucleotide dissociation in *E. coli* DnaK[39]. In the structure of bovine Hsc70 complexed with yeast Sse1,[32] the salt bridge formed by K56 and E268 is disrupted by the rotation of subdomain IIB, which might facilitate nucleotide exchange. Modification of subdomains IB and IIB by Apg2 C-terminal extension might partially stabilize existing links across the interface between lobe I and II of Hsc70 NBD, or add more, to hamper opening of the nucleotide binding cleft and, thus, slow nucleotide exchange.

Another important result in this work is that Apg2 C-terminal extension increases the affinity of the Hsc70:Apg2 complex in a nucleotide dependent manner: the K_d of the complex changed from approximately 150 nM for the proteins in the apo state, to 2 nM when Hsc70 and Apg2 were mixed in the presence of ATP and incubated to allow nucleotide hydrolysis. In contrast, only a slight affinity gain was found for Apg2ΔC, with a K_d of 151 nM in the absence of nucleotides and 100 nM upon ATP hydrolysis. These affinity changes strongly suggest that the interaction of Apg2 C-terminal extension with Hsc70 NBD depends on a nucleotide-induced conformational change. Taking into account that in the high affinity complex (after ATP hydrolysis) Hsc70 is in the ADP state and the fact that Apg2 and Hsc70 interact with very low affinity in the ADP conformation[11], the conformational rearrangement resulting in the stabilization of the Hsc70:Apg2 complex should be attributed to Apg2. This conformational change possibly affects the helical segment of the C-terminal extension, as the main responsible for affinity regulation, although minor stabilizing effects due to modification of the IDR should not be discarded. However, we did not observe any significant conformational change upon nucleotide binding to isolated Apg2 by partial proteolysis, as previously reported,[15] and differential IR. An alternative possibility is that the ATP-dependent rearrangement of the C-terminal extension senses both Apg2 binders, ATP and Hsc70, to interact with the NBD of the latter. The lack of high-resolution structural data of human Apg2 and/or its complex with Hsc70 does not provide evidence to support this hypothesis. The Alphafold prediction for human Apg2 shows the structured 3-helix bundle of the C-terminal extension connected by a bent α-helix to the other helical bundle that precedes it in the SBDα. Bending of this helix might act as a hinge allowing movement of the C-terminal bundle to stabilize the interaction with the NBD of Hsc70.

The absolute *in vivo* concentration of human chaperones is unknown but Apg2 is around 10 to 30 times less abundant than Hsc70 under normal conditions.[56–57] At roughly similar Hsc70:Apg2 ratios, the mutant Apg2ΔC has proven to be a more efficient NEF for Hsc70 than the wt protein, promoting faster reactivation of protein aggregates *in vitro*.

This raises an intriguing question: why human Hsp110 proteins have a long C-terminal extension instead of a shorter sequence like that of yeast Sse1? In the cellular milieu, the pool of Hsc70 molecules has to perform many different tasks and free Hsc70 might be scarce. In this situation, it is very likely that a high affinity interaction with Hsc70, provided by the helical segment of the C-terminal extension, is essential to stimulate optimal refolding of protein aggregates. Yeast might live with a lower affinity Hsp70:Hsp110 complex[30–31], as aggregate reactivation occurs in cooperation with the potent disaggregase Hsp104. Also, the IDR present in the C-terminal extension could be important to provide Apg2 with a potent holdase activity required *in vivo* to avoid protein aggregation[21], and it might also play a role in other less known functions of Apg2 essential for cellular fitness[3]. Taking together the results in this work and our previous report on the role of the AS[11], we found that the two divergent domains in human Apg2 fine-tune the chaperone activity of Hsc70, tinkering with the ATPase cycle. Importantly, post-translational modifications in Apg2 C-terminal extension[22–24] could regulate the interaction with Hsc70 NBD to further optimize its role as a fine-tuner of the Hsc70 system activity in different physiological conditions.

Materials and Methods

Cloning, expression and purification of proteins

Apg2 (HSPH2), full length Hsc70 (HSPA8) and DnaJB1 were expressed and purified as described.[11] The mutants Apg2ΔC and Apg2ΔIDR, carrying the deletion of residues from L702 to D840 and P781 to D840, respectively, were cloned by PCR into pE-SUMO vector (LifeSensors). Apg2ΔC and Apg2ΔIDR were purified following the same protocol used for wt Apg2.

Circular dichroism

Spectra were obtained at 2.5 μM protein concentration in 15 mM Hepes-KOH, pH 7.6, 50 mM potassium acetate, 2 mM magnesium acetate, 2 mM DTT. 10 spectra were recorded in a 1 mm path length cuvette and averaged, using a JASCO J-8100 spectropolarimeter (Jasko, Tokio, Japan).

Small angle X-ray scattering measurements

Synchrotron X-ray diffraction data for recombinant purified Apg2ΔC were collected on a pixel Pilatus 2M detector at Diamond Light Source B21 beamline (UK). The scattering patterns were measured with a 2-s exposure time per frame in a continuous mode using an in-line Agilent HPLC system connected to a SHODEX PROTEIN KW403-4F column (exclusion limit of 600 kDa) equilibrated in 40 mM HEPES pH 7.6, 150 mM KCl, 5 mM $MgCl_2$ and 2 mM DTT and running at 0.16 ml min^{-1}. To check for radiation damage, the accumulated frames corresponding to eluted peaks were compared as a time-series and no radiation damage was observed. Using the sample-to-detector distance of 4.01 m, the range of momentum transfer values is $0.0025 < q < 0.42$ $Å^{-1}$ ($q = 4\pi \sin(\theta)/\lambda$ where 2θ is the scattering angle and $\lambda = 1$ Å is the X-ray wavelength). Data were processed using standard procedures by the program packages ScÅtter (developed by Rob Rambo at Diamond Light Source). The forward scattering ($I(0)$) was evaluated using the Guinier approximation[58] assuming the intensity is represented as $I(q) = I(0)\exp(-(qR_g)^2/3)$ for a very small range of momentum transfer values ($q < 1.3/R_g$). The maximum dimensions (D_{max}), the interatomic distance distribution functions ($P(r)$), and the radii of gyration (R_g) were computed using GNOM.[59] The molecular mass of the protein was evaluated with the equation $ln(Q_R) = k * ln(MW) + c$, where $Q_R = (V_c^2/R_g)$, and k and c are constants[60](Supplemental Table 1).

Ab initio shape determination

The *ab-initio* reconstruction of Apg2ΔC was calculated using GASBOR,[61] and MONSA[62] for the overall fit using wt Apg2 data.[11] Structure clustering and averaging were carried out with DAMCLUST.[63] Representative *ab-initio* reconstructions were selected based on DAMCLUST results.

Surface plasmon resonance spectroscopy (SPR)

SPR assays were performed in a Biacore 3000 system (GE Healthcare), using CM5 chips (GE Healthcare) coated with Hsc70 carrying a C-terminal strep-tag II as described.[11] Apg2 or Apg2ΔC, dialyzed overnight at 4 °C in running buffer (40 mM Hepes, pH 7.5, 150 mM KCl, 5 mM $MgCl_2$ and 0.0025% Tween 20), were injected for 1 min at concentrations from 0.01 to 10 μM. Undissociated Apg2 and Apg2ΔC were washed away after every injection passing a solution containing 1 M NaCl through the flow cells for 1 min. Measurements temperature was 25 °C and flow rate 30 μl/min. Double subtraction of buffer and control (injection of Apg2 or Apg2ΔAS along a flow cell without Hsc70) was done. The maximal value of RU achieved was plotted as a function of Hsp110 concentration injected and K_ds were determined by fitting to a hyperbolic ligand-binding equation.

Native gel electrophoresis

Binding competition experiments were performed by mixing Hsc70 (2 μM) with Apg2 (2 μM) and Apg2ΔC or Apg2ΔIDR (0–10 μM) in 40 mM Hepes, pH 7.6, 50 mM KCl, 5 mM $MgCl_2$, 2 mM

DTT, 50 μM ATP. Reverse titrations were performed with Hsc70 (2 μM), Apg2ΔC or Apg2ΔIDR (2 μM) and Apg2 (0–10 μM) Samples were incubated overnight at room temperature. Complexes were resolved by native PAGE using 4–16% Bis-Tris gels (Invitrogen) and stained with Coomassie blue. Assuming that the three proteins in complex stain similarly, the molar ratios of Hsc70 bound to Apg2, Apg2ΔC or Apg2ΔIDR were obtained from densitometry of the corresponding bands. To convert the optical density into a molar fraction, the different molecular weight of each complex was taken into account and total Hsc70 was estimated by adding the densities of the two complexes at high concentrations of wt Apg2 (>5 μM), i.e., when virtually all Hsc70 molecules are complexed with Apg2. This assumes that free Hsc70 is negligible under these conditions, which is reasonable considering the expected affinity of Apg2 and the deletion mutants for Hsc70, at least similar to those estimated in the absence of nucleotides (∼150 nM). This method solves the troublesome quantification of Hsc70, due to the existence of different oligomeric forms. The fractions of Hsc70:Apg2ΔC or Hsc70:Apg2ΔIDR complexes at increasing wt Apg2 concentrations were fitted using the solution to Eq. (6) in Origin 7.

Chemical shift perturbation analysis by NMR

Hsc70 NBD (residues 1–384) was labeled with ^{15}N by expressing the protein in *E. coli* Rossetta cells grown in M9 minimal medium supplemented with $^{15}NH_4Cl$ (Sigma-Aldrich, 299251), and purified as described.[11] NMR experiments were performed on a Bruker Avance III 800 MHz spectrometer equipped with a triple resonance ^{1}H, ^{13}C, ^{15}N-cryoprobe. Two-dimensional ^{1}H-^{15}N TROSY spectra were recorded at 298 K for 1 h using 150 μM ^{15}N-labelled NBD Hsc70 protein (signal reporter) in a final volume of 500 μl, in the presence of 500 μM ATP. Apg2 or Apg2ΔC were added at 75 μM. All the samples were incubated for 12 h at room temperature before NMR measurement. Reference chemical shifts values were obtained from BMRB entry 26815.[38] The assignment was done using CCP NMR software. Chemical shift and peak intensity values were extracted for each titration point. All this information was analyzed with different in-house MatLab scripts. Peak intensity analysis includes the signal lost from the complex formation and the signal broadening from the chemical shift perturbation.

Nucleotide exchange

Stopped-flow measurements of nucleotide exchange were performed in a SFM 300 / MOS 450 machine (BioLogic, Grenoble, France). Hsc70-MABA-ADP preformed complexes were mixed with ATP in the presence of increasing concentrations of Apg2, Apg2ΔC or Apg2ΔIDR to obtain final reactants concentrations: 0.48 μM Hsc70-MABA-ADP, 268.5 μM ATP, and 0 to 0.4 μM Hsp110 in 40 mM Hepes, pH 7.6, 50 mM KCl, 5 mM $MgCl_2$. The average mixing-time of the experiment was 80 ms. ATP and Hsp110 proteins were injected from separate syringes, to avoid ATP hydrolysis during the measurements, and were premixed for 5 s before mixing with Hsc70(MABA-ADP). Various premixing times of Apg2 with ATP, from 30 ms to 30 s, were assayed, resulting in identical MABA-ADP exchange kinetics. MABA-ADP release was recorded immediately after mixing as a decrease in its fluorescence signal, upon excitation at 365 nm and selection of the emitted light with a 400 nm cut-off filter. The cell chamber and container syringes were kept at 25 °C. Kinetic constants were calculated by fitting the experimental traces to a mono-exponential transition by means of the Bio-Kine32 v4.65 analysis software provided by Biologic.

ATPase measurements

Steady-state ATPase activity was measured at 30 °C in 40 mM Hepes, pH 7.6, 50 mM KCl, 5 mM magnesium acetate, 1 mM ATP, following a described method.[64] Protein concentrations were 2 μM Hsc70, 0.5 μM DnaJB1, 0–5 μM Apg2 or Apg2ΔC. Reactions were monitored by continuously measuring the absorbance decay at 340 nm for 1 h at 30 °C in a Synergy HTX plate reader (Biotec).

Refolding of luciferase and G6PDH aggregates

Luciferase (2 μM) was denatured by incubation at 30 °C for 30 min in 6 M urea, 40 mM Hepes, pH 7.6, 50 mM KCl, 5 mM $MgCl_2$, 2 mM DTT. Denatured luciferase was diluted 100-fold into refolding buffer (40 mM Hepes, pH 7.6, 50 mM KCl, 5 mM $MgCl_2$, 2 mM DTT, 2 mM ATP, 3 mM PEP, 20 ng/ml Pyruvate Kinase) to induce aggregation. G6PDH (Glucose-6-phosphate dehydrogenase) (2.5 μM) aggregation was induced by heating at 50 °C for 30 min in 50 mM Tris-HCl, pH 7.5, 150 mM KCl, 20 mM $MgCl_2$, 10 mM DTT. Then, G6PDH was diluted to 0.4 μM in refolding buffer and preincubated at 30 °C for 10 min. Different combinations of Hsc70 (2 μM) and DnaJB1 (1 μM) with variable concentrations of Apg2, Apg2ΔC or Apg2ΔIDR (0–8 μM) were used to reactivate the aggregates. To obtain reactivation rates, aliquots were taken at different times during 2 h and the activity of luciferase and G6PDH was measured as described.[11] The initial linear part of the refolding kinetic was fitted to a linear regression to obtained reactivation rates.

Declaration of interest

None.

CRediT authorship contribution statement

Yovana Cabrera: Investigation, Formal analysis, Visualization. **Ganeko Bernardo-Seisdedos:** Investigation, Methodology, Formal analysis, Visualization, Writing – review & editing. **Leire Dublang:** Investigation. **David Albesa-Jové:** Investigation, Formal analysis, Visualization. **Natalia Orozco:** Investigation, Resources. **Ana Rosa Viguera:** Investigation, Formal analysis. **Oscar Millet:** Conceptualization, Methodology. **Arturo Muga:** Conceptualization, Methodology, Writing – review & editing, Funding acquisition. **Fernando Moro:** Conceptualization, Methodology, Visualization, Writing – original draft, Writing – review & editing, Funding acquisition.

DATA AVAILABILITY

Data will be made available on request.

Acknowledgements

The authors thankfully acknowledge the NMR resources and technical support provided by the LRE node of the Spanish ICTS Red de Laboratorios de RMN de Biomoléculas (R_LRB), and Diamond Light Source (proposals sm21035), and the B21 beamline staff, including Dr. Robert Rambo, for assistance with SAXS data collection Y.C. and L.D. were recipients of UPV/EHU and MEC FPU predoctoral fellowships, respectively. We thank Fundación Biofisika Bizkaia for supporting N.O. This work was supported by CTQ2016-76941-R (MINECO), Fundación Biofísica Bizkaia, the Basque Excellence Research Centre (BERC) of the Basque Government and Fundación BBVA to D.A.-J., and BFU2016-75983-P and PID2019-111068 GB-100 (MCI/AEI/FEDER, UE) grants from Spanish Government to A.M. and F.M. and IT1745-22 from Basque Government to F.M.

Appendix A. Supplementary Data

Supplementary data to this article can be found online at https://doi.org/10.1016/j.jmb.2022.167841.

Received 26 May 2022;
Accepted 21 September 2022;
Available online 24 September 2022

Keywords:
Hsc70;
Apg2;
chaperone complex;
chaperone regulation;
protein aggregation

† Present address: Department of Chemistry and Molecular Biology, University of Gothenburg, Medicinaregatan 9C, 41390 Gothenburg, Sweden.

References

1. Vos, M.J., Hageman, J., Carra, S., Kampinga, H.H., (2008). Structural and functional diversities between members of the human HSPB, HSPH, HSPA, and DNAJ chaperone families. *Biochemistry* **47**, 7001–7011.
2. Balchin, D., Hayer-Hartl, M., Hartl, F.U., (2016). In vivo aspects of protein folding and quality control. *Science* **353**, aac4354.
3. Aguado, A., Fernandez-Higuero, J.A., Moro, F., Muga, A., (2015). Chaperone-assisted protein aggregate reactivation: Different solutions for the same problem. *Arch. Biochem. Biophys.* **580**, 121–134.
4. Yamagishi, N., Goto, K., Nakagawa, S., Saito, Y., Hatayama, T., (2010). Hsp105 reduces the protein aggregation and cytotoxicity by expanded-polyglutamine proteins through the induction of Hsp70. *Exp. Cell Res.* **316**, 2424–2433.
5. Yamagishi, N., Ishihara, K., Saito, Y., Hatayama, T., (2003). Hsp105 but not Hsp70 family proteins suppress the aggregation of heat-denatured protein in the presence of ADP. *FEBS Lett.* **555**, 390–396.
6. Oh, H.J., Chen, X., Subjeck, J.R., (1997). Hsp110 protects heat-denatured proteins and confers cellular thermoresistance. *J. Biol. Chem.* **272**, 31636–31640.
7. Dragovic, Z., Broadley, S.A., Shomura, Y., Bracher, A., Hartl, F.U., (2006). Molecular chaperones of the Hsp110 family act as nucleotide exchange factors of Hsp70s. *EMBO J.* **25**, 2519–2528.
8. Andreasson, C., Fiaux, J., Rampelt, H., Mayer, M.P., Bukau, B., (2008). Hsp110 is a nucleotide-activated exchange factor for Hsp70. *J. Biol. Chem.* **283**, 8877–8884.
9. Rampelt, H., Kirstein-Miles, J., Nillegoda, N.B., Chi, K., Scholz, S.R., Morimoto, R.I., (2012). Metazoan Hsp70 machines use Hsp110 to power protein disaggregation. *EMBO J.* **31**, 4221–4235.
10. Gao, X., Carroni, M., Nussbaum-Krammer, C., Mogk, A., Nillegoda, N.B., Szlachcic, A., (2015). Human Hsp70 Disaggregase Reverses Parkinson's-Linked alpha-Synuclein Amyloid Fibrils. *Mol. Cell* **59**, 781–793.
11. Cabrera, Y., Dublang, L., Fernandez-Higuero, J.A., Albesa-Jove, D., Lucas, M., Viguera, A.R., (2019). Regulation of Human Hsc70 ATPase and Chaperone Activities by Apg2: Role of the Acidic Subdomain. *J. Mol. Biol.* **431**, 444–461.
12. Nillegoda, N.B., Bukau, B., (2015). Metazoan Hsp70-based protein disaggregases: emergence and mechanisms. *Front Mol Biosci.* **2**, 57.
13. Wentink, A.S., Nillegoda, N.B., Feufel, J., Ubartaite, G., Schneider, C.P., De Los Rios, P., (2020). Molecular dissection of amyloid disaggregation by human HSP70. *Nature* **587**, 483–488.
14. Franco, A., Gracia, P., Colom, A., Camino, J.D., Fernandez-Higuero, J.A., Orozco, N., et al., (2021). All-or-none amyloid disassembly via chaperone-triggered fibril unzipping favors clearance of alpha-synuclein toxic species. *Proc. Natl. Acad. Sci. U. S. A.* **118** e2105548118.

15. Raviol, H., Bukau, B., Mayer, M.P., (2006). Human and yeast Hsp110 chaperones exhibit functional differences. *FEBS Lett.* **580**, 168–174.
16. Andreasson, C., Fiaux, J., Rampelt, H., Druffel-Augustin, S., Bukau, B., (2008). Insights into the structural dynamics of the Hsp110-Hsp70 interaction reveal the mechanism for nucleotide exchange activity. *Proc. Natl. Acad. Sci. U. S. A.* **105**, 16519–16524.
17. Liu, Q., Hendrickson, W.A., (2007). Insights into Hsp70 chaperone activity from a crystal structure of the yeast Hsp110 Sse1. *Cell* **131**, 106–120.
18. Kityk, R., Kopp, J., Sinning, I., Mayer, M.P., (2012). Structure and dynamics of the ATP-bound open conformation of Hsp70 chaperones. *Mol. Cell* **48**, 863–874.
19. Saito, Y., Yamagishi, N., Hatayama, T., (2007). Different localization of Hsp105 family proteins in mammalian cells. *Exp. Cell Res.* **313**, 3707–3717.
20. Saito, Y., Yamagishi, N., Hatayama, T., (2009). Nuclear localization mechanism of Hsp105beta and its possible function in mammalian cells. *J. Biochem.* **145**, 185–191.
21. Yakubu, U.M., Morano, K.A., (2021). Suppression of aggregate and amyloid formation by a novel intrinsically disordered region in metazoan Hsp110 chaperones. *J. Biol. Chem.* **296**, 100567
22. Velasco, L., Dublang, L., Moro, F., Muga, A., (2019). The Complex Phosphorylation Patterns that Regulate the Activity of Hsp70 and Its Cochaperones. *Int. J. Mol. Sci.* **20**, 4122.
23. Akimov, V., Barrio-Hernandez, I., Hansen, S.V.F., Hallenborg, P., Pedersen, A.K., Bekker-Jensen, D.B., (2018). UbiSite approach for comprehensive mapping of lysine and N-terminal ubiquitination sites. *Nat. Struct. Mol. Biol.* **25**, 631–640.
24. Wagner, S.A., Beli, P., Weinert, B.T., Nielsen, M.L., Cox, J., Mann, M., (2011). A proteome-wide, quantitative survey of in vivo ubiquitylation sites reveals widespread regulatory roles. *Mol. Cell. Proteomics* **10**, (M111) 013284
25. Drozdetskiy, A., Cole, C., Procter, J., Barton, G.J., (2015). JPred4: a protein secondary structure prediction server. *Nucleic Acids Res.* **43**, W389–W394.
26. Dublang, L., Underhaug, J., Flydal, M.I., Velasco-Carneros, L., Maréchal, J.-D., Moro, F., (2021). Inhibition of the Human Hsc70 System by Small Ligands as a Potential Anticancer Approach. *Cancers (Basel).* **13**, 2936.
27. Zhang, P., Leu, J.I., Murphy, M.E., George, D.L., Marmorstein, R., (2014). Crystal structure of the stress-inducible human heat shock protein 70 substrate-binding domain in complex with peptide substrate. *PLoS ONE* **9**, e103518.
28. Jumper, J., Evans, R., Pritzel, A., Green, T., Figurnov, M., Ronneberger, O., (2021). Highly accurate protein structure prediction with AlphaFold. *Nature* **596**, 583–589.
29. Varadi, M., Anyango, S., Deshpande, M., Nair, S., Natassia, C., Yordanova, G., (2022). AlphaFold Protein Structure Database: massively expanding the structural coverage of protein-sequence space with high-accuracy models. *Nucleic Acids Res.* **50**, D439–D444.
30. Polier, S., Dragovic, Z., Hartl, F.U., Bracher, A., (2008). Structural basis for the cooperation of Hsp70 and Hsp110 chaperones in protein folding. *Cell* **133**, 1068–1079.
31. Raviol, H., Sadlish, H., Rodriguez, F., Mayer, M.P., Bukau, B., (2006). Chaperone network in the yeast cytosol: Hsp110 is revealed as an Hsp70 nucleotide exchange factor. *EMBO J.* **25**, 2510–2518.
32. Schuermann, J.P., Jiang, J., Cuellar, J., Llorca, O., Wang, L., Gimenez, L.E., (2008). Structure of the Hsp110:Hsc70 nucleotide exchange machine. *Mol. Cell* **31**, 232–243.
33. Lacabanne, D., Wiegand, T., Wili, N., Kozlova, M.I., Cadalbert, R., Klose, D., (2020). ATP Analogues for Structural Investigations: Case Studies of a DnaB Helicase and an ABC Transporter. *Molecules* **25**, 5268.
34. Yan, X., Shi, Q., Bracher, A., Milicic, G., Singh, A.K., Hartl, F.U., (2018). GroEL Ring Separation and Exchange in the Chaperonin Reaction. *Cell* **172** (605–617), e611.
35. Wang, Z.X., (1995). An exact mathematical expression for describing competitive binding of two different ligands to a protein molecule. *FEBS Lett.* **360**, 111–114.
36. von Germar, F., Galan, A., Llorca, O., Carrascosa, J.L., Valpuesta, J.M., Mantele, W., (1999). Conformational changes generated in GroEL during ATP hydrolysis as seen by time-resolved infrared spectroscopy. *J. Biol. Chem.* **274**, 5508–5513.
37. Moro, F., Fernandez-Saiz, V., Muga, A., (2006). The allosteric transition in DnaK probed by infrared difference spectroscopy. Concerted ATP-induced rearrangement of the substrate binding domain. *Protein Sci.* **15**, 223–233.
38. Zuiderweg, E.R., Gestwicki, J.E., (2017). Backbone and methyl resonance assignments of the 42 kDa human Hsc70 nucleotide binding domain in the ADP state. *Biomol NMR Assign.* **11**, 11–15.
39. Brehmer, D., Rudiger, S., Gassler, C.S., Klostermeier, D., Packschies, L., Reinstein, J., (2001). Tuning of chaperone activity of Hsp70 proteins by modulation of nucleotide exchange. *Nat. Struct. Biol.* **8**, 427–432.
40. Ung, P.M., Thompson, A.D., Chang, L., Gestwicki, J.E., Carlson, H.A., (2013). Identification of key hinge residues important for nucleotide-dependent allostery in E. coli Hsp70/DnaK. *PLoS Comput. Biol.* **9**, e1003279.
41. Zhuravleva, A., Gierasch, L.M., (2011). Allosteric signal transmission in the nucleotide-binding domain of 70-kDa heat shock protein (Hsp70) molecular chaperones. *Proc. Natl. Acad. Sci. U. S. A.* **108**, 6987–6992.
42. Kityk, R., Kopp, J., Mayer, M.P., (2018). Molecular Mechanism of J-Domain-Triggered ATP Hydrolysis by Hsp70 Chaperones. *Mol. Cell* **69** (227–237), e224.
43. Shaner, L., Trott, A., Goeckeler, J.L., Brodsky, J.L., Morano, K.A., (2004). The function of the yeast molecular chaperone Sse1 is mechanistically distinct from the closely related hsp70 family. *J. Biol. Chem.* **279**, 21992–22001.
44. Gassler, C.S., Wiederkehr, T., Brehmer, D., Bukau, B., Mayer, M.P., (2001). Bag-1M accelerates nucleotide release for human Hsc70 and Hsp70 and can act concentration-dependent as positive and negative cofactor. *J. Biol. Chem.* **276**, 32538–32544.
45. Tzankov, S., Wong, M.J., Shi, K., Nassif, C., Young, J.C., (2008). Functional divergence between co-chaperones of Hsc70. *J. Biol. Chem.* **283**, 27100–27109.
46. Packschies, L., Theyssen, H., Buchberger, A., Bukau, B., Goody, R.S., Reinstein, J., (1997). GrpE accelerates nucleotide exchange of the molecular chaperone DnaK with an associative displacement mechanism. *Biochemistry* **36**, 3417–3422.
47. Zhang, Y., Zuiderweg, E.R., (2004). The 70-kDa heat shock protein chaperone nucleotide-binding domain in solution unveiled as a molecular machine that can reorient its functional subdomains. *Proc. Natl. Acad. Sci. U. S. A.* **101**, 10272–10277.

48. Vogel, M., Bukau, B., Mayer, M.P., (2006). Allosteric regulation of Hsp70 chaperones by a proline switch. *Mol. Cell* **21**, 359–367.
49. Sondermann, H., Scheufler, C., Schneider, C., Hohfeld, J., Hartl, F.U., Moarefi, I., (2001). Structure of a Bag/Hsc70 complex: convergent functional evolution of Hsp70 nucleotide exchange factors. *Science* **291**, 1553–1557.
50. Yan, M., Li, J., Sha, B., (2011). Structural analysis of the Sil1-Bip complex reveals the mechanism for Sil1 to function as a nucleotide-exchange factor. *Biochem. J.* **438**, 447–455.
51. Flaherty, K.M., DeLuca-Flaherty, C., McKay, D.B., (1990). Three-dimensional structure of the ATPase fragment of a 70K heat-shock cognate protein. *Nature* **346**, 623–628.
52. Huang, S.P., Tsai, M.Y., Tzou, Y.M., Wu, W.G., Wang, C., (1993). Aspartyl residue 10 is essential for ATPase activity of rat hsc70. *J. Biol. Chem.* **268**, 2063–2068.
53. Rajapandi, T., Wu, C., Eisenberg, E., Greene, L., (1998). Characterization of D10S and K71E mutants of human cytosolic hsp70. *Biochemistry* **37**, 7244–7250.
54. Russell, R., Jordan, R., McMacken, R., (1998). Kinetic characterization of the ATPase cycle of the DnaK molecular chaperone. *Biochemistry* **37**, 596–607.
55. Siegenthaler, R.K., Christen, P., (2006). Tuning of DnaK chaperone action by nonnative protein sensor DnaJ and thermosensor GrpE. *J. Biol. Chem.* **281**, 34448–34456.
56. Hageman, J., van Waarde, M.A., Zylicz, A., Walerych, D., Kampinga, H.H., (2011). The diverse members of the mammalian HSP70 machine show distinct chaperone-like activities. *Biochem. J.* **435**, 127–142.
57. Finka, A., Sharma, S.K., Goloubinoff, P., (2015). Multi-layered molecular mechanisms of polypeptide holding, unfolding and disaggregation by HSP70/HSP110 chaperones. *Front Mol Biosci.* **2**, 29.
58. Guinier, A., (1939). La diffraction des rayons X aux très petits angles : application à l'étude de phénomènes ultramicroscopiques. *Ann. Phys.* **11**, 161–237.
59. Svergun, D.I., (1992). Determination of the regularization parameter in indirect-transform methods using perceptual criteria. *J. Appl. Crystallogr.* **25**, 495–503.
60. Rambo, R.P., Tainer, J.A., (2013). Accurate assessment of mass, models and resolution by small-angle scattering. *Nature* **496**, 477–481.
61. Franke, D., Svergun, D.I., (2009). DAMMIF, a program for rapid ab-initio shape determination in small-angle scattering. *J. Appl. Crystallogr.* **42**, 342–346.
62. Svergun, D.I., (1999). Restoring low resolution structure of biological macromolecules from solution scattering using simulated annealing. *Biophys. J .* **76**, 2879–2886.
63. Petoukhov, M.V., Franke, D., Shkumatov, A.V., Tria, G., Kikhney, A.G., Gajda, M., (2012). New developments in the ATSAS program package for small-angle scattering data analysis. *J. Appl. Crystallogr.* **45**, 342–350.
64. Norby, J.G., (1988). Coupled assay of Na+, K+-ATPase activity. *Methods Enzymol.* **156**, 116–119.